

Injecting solid particles into the stratosphere could mitigate global warming but currently entails great uncertainties

Vattioni, Sandro; Peter, Thomas; Weber, Rahel; Dykema, John A.; Luo, Beiping; Stenke, Andrea; Feinberg, Aryeh; Sukhodolov, Timofei; Kelesidis, Georgios A.; More Authors

DOI

[10.1038/s43247-025-02038-1](https://doi.org/10.1038/s43247-025-02038-1)

Publication date

2025

Document Version

Final published version

Published in

Communications Earth and Environment

Citation (APA)

Vattioni, S., Peter, T., Weber, R., Dykema, J. A., Luo, B., Stenke, A., Feinberg, A., Sukhodolov, T., Kelesidis, G. A., & More Authors (2025). Injecting solid particles into the stratosphere could mitigate global warming but currently entails great uncertainties. *Communications Earth and Environment*, 6(1), Article 132. <https://doi.org/10.1038/s43247-025-02038-1>

Important note

To cite this publication, please use the final published version (if applicable). Please check the document version above.

Copyright

Other than for strictly personal use, it is not permitted to download, forward or distribute the text or part of it, without the consent of the author(s) and/or copyright holder(s), unless the work is under an open content license such as Creative Commons.

Takedown policy

Please contact us and provide details if you believe this document breaches copyrights. We will remove access to the work immediately and investigate your claim.

<https://doi.org/10.1038/s43247-025-02038-1>

Injecting solid particles into the stratosphere could mitigate global warming but currently entails great uncertainties

Check for updates

Sandro Vattioni ^{1,2}✉, Thomas Peter ¹, Rahel Weber ^{1,2,11}, John A. Dykema ², Beiping Luo ¹, Andrea Stenke ^{1,3,4}, Aryeh Feinberg ^{1,3,12}, Timofei Sukhodolov ⁵, Frank N. Keutsch ^{2,6,7}, Markus Ammann ⁸, Christof Vockenhuber ⁹, Max Döbeli ⁹, Georgios A. Kelesidis ^{10,13} & Gabriel Chiodo ^{1,14}

Stratospheric aerosol injection could mitigate harmful effects of global warming, but could have undesirable side effects, such as warming the stratosphere and depleting the ozone layer. We explore the potential benefits of solid alumina and calcite particles as alternatives to sulfate aerosols by using an experimentally informed aerosol-chemistry-climate model. Compared to sulfur dioxide, injection of solids reduces stratospheric warming by up to 70% and diffuse radiation by up to 40%, highlighting their potential benefits. Achieving -1 W m^{-2} of radiative forcing would likely result in very small ozone changes, but sizable uncertainties remain. These arise from poorly understood heterogeneous chemical and microphysical processes, which, under less likely assumptions, could lead to larger global ozone column changes between -14% and $+4\%$. Our work provides recommendations for improving the understanding of stratospheric aerosol injection using materials other than sulfur dioxide, and underscores the need for kinetic laboratory studies.

As a supplement to emission reduction, stratospheric aerosol injection (SAI) has been proposed as a climate intervention that could help to rapidly mitigate some of the most harmful effects of climate change^{1,2}. SAI could potentially help meet the Paris agreement by keeping global warming below 1.5 K, until net-zero greenhouse gas (GHG) emissions are reached and GHG removal techniques are developed and scaled up^{3,4}. The idea developed from observations of the cooling effect of explosive volcanic eruptions. Volcanic analogues are also the reason why research on SAI has so far focused on the injection of gaseous sulfur dioxide (SO_2), a major precursor of aqueous sulfuric acid droplets in the stratosphere^{5–7}. Due to their natural occurrence, the microphysics, optical properties, and heterogeneous chemistry of stratospheric sulfuric acid aerosols are relatively well-studied and understood^{5,6,8,9}. However, there is evidence that sulfur-based SAI could come along with a number of serious side effects^{10–14}. Some adverse SAI effects could potentially be alleviated by injecting materials such as alumina (Al_2O_3) or calcite (CaCO_3) instead of sulfurous species^{15,16}, as these solid particles absorb less terrestrial infrared radiation and scatter solar radiation better. The improved ability to scatter solar light implies that less stratospheric aerosol loading is needed^{15,17–22}, which would reduce the SAI-

induced enhancement of diffuse radiation, possibly reducing potential modulation of plant ecology and ecosystem productivity^{23,24}. Most importantly, these materials could also lead to less aerosol-induced heating of the stratosphere^{15,19}, which is known to considerably perturb global atmospheric dynamics and regional precipitation patterns^{11–14,25–27}. Furthermore, the sizable stratospheric ozone loss in the southern hemisphere caused by sulfur-based SAI^{28–31} could potentially be mitigated by solid particles with lower surface area densities and chemically more inert properties, limiting the heterogeneous chemistry on their surfaces^{32–34}.

Previous attempts to model solid particle SAI have been limited by simplified configurations that, for example, neglect the microphysical and chemical interactions between solid particles and stratospheric composition^{17–20} or did not account for interactions between particles, transport and radiation^{15,35}. Here we employ the sectional aerosol-chemistry-climate model (ACCM) SOCOL-AERv2 (Solar Climate Ozone Links-Atmospheric and Environmental Research Incorporation version 2)⁷ and expand it to interactively simulate the injection of solid particles, their microphysical interactions and heterogeneous chemistry, as well as their interactions with transport and radiation³⁴ (see Methods). These processes

A full list of affiliations appears at the end of the paper. ✉e-mail: sandro.vattioni@env.ethz.ch

were missing in previous studies and are crucial to realistically simulate the impacts of SAI via solid particles. Using experimentally determined parameters in combination with these novel and unprecedented modeling capabilities, our assessment of the uncertainties, risks and benefits of SAI of solid particles compared to sulfur-based SAI fills a gap highlighted in the World Meteorological Organization's recent Scientific Assessment of Ozone Depletion: "Comprehensive climate model simulations to quantify these effects [of solid aerosols] have yet to be performed"¹⁰.

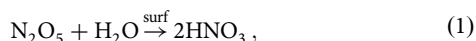
Results

We performed four simulations in which 5 Mt yr⁻¹ (Megatons per year) of material is injected either as gaseous SO₂ or aqueous sulfuric acid aerosol in the accumulation mode (AM – H₂SO₄, log-normally distributed with $r_m = 0.095 \mu\text{m}$ and $\sigma = 1.5$) or mono-disperse calcite or alumina particles with a radius of 240 nm, which is close to the optimal radius for back-scattering solar radiation¹⁹. The injection, e.g., by high-flying airplanes, is assumed to be at 50 hPa (about 20 km), homogeneously distributed within all model grid boxes (i.e., about 325 km × 325 km × 1.5 km resolution) between 30°N and 30°S, from where the material is transported all over the globe by the atmospheric circulation.

SAI microphysics and heterogeneous chemistry

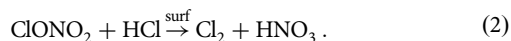
In the model, the aerosols undergo nucleation and condensation/evaporation, self-coagulation and coagulation with the natural stratospheric background aerosol, chemical processing and gravitational settling. Concentrations of GHGs and ozone depleting substances (ODS) and sea surface temperatures (SST) are assumed for the years 2020 or 2090 (see Methods).

The model calculates stratospheric particle size distributions and heterogeneous chemical reactions on the particle surfaces fully kinetically (see supplementary Notes 1 and Supplementary Fig. 1). On aqueous H₂SO₄ droplets the dominant reaction in the tropics and mid-latitudes is



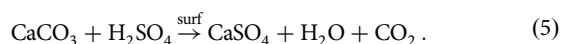
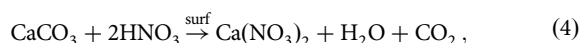
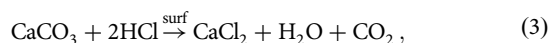
which leads to nitrogen deactivation, while in the cold regions of the polar winter vortices or close to the tropical tropopause, heterogeneous chlorine and bromine activation reactions are important³⁶. All of these have major impacts on the ozone layer.

For alumina particles, which can accommodate aqueous sulfuric acid on their surface via condensation of gaseous H₂SO₄ and coagulation with aqueous H₂SO₄ droplets, we found a contact angle of about 30°³³, leaving part of their surface uncovered. While the heterogeneous chemistry on the H₂SO₄-covered parts is treated in the same way as on sulfuric acid aerosols, the most important reaction on bare aluminum oxide is



Most probably the uptake of HCl is dissociative, leading to H₃O⁺ and Cl⁻, and is reduced by competitive HNO₃ coadsorption. While this is plausible, it currently remains speculative and is associated with very large uncertainties that may have a critical impact on stratospheric ozone³³.

For calcite particles the following heterogeneous reactions are important:



These reactions not only remove reservoir gases of ozone-destroying radicals, but also convert calcite into other calcium compounds with different radiative and chemical properties. The best estimates for the

reactive uptake coefficients associated with Reactions (3–5) are currently $\gamma_{\text{HCl}} = 10^{-5}$, $\gamma_{\text{HNO}_3} = 10^{-4}$, and $\gamma_{\text{H}_2\text{SO}_4} = 1$ ^{21,34,37}. These are realistic but highly uncertain because they must take into account the dependence on the exposure of the particles to stratospheric HCl and HNO₃ concentrations³⁴.

Solid particles may reduce some SAI side effects

With SAI, the aim is to induce a negative radiative forcing (RF, in W m⁻²), reducing the imbalance created by anthropogenic GHG emissions. Therefore, the efficacy of different SAI materials and the reduction of their side effects should be compared with respect to the same negative net all sky top of the atmosphere (ToA) RF. Figure 1 shows the results of four 45-year time slice simulations for gaseous, liquid and solid materials introduced into the stratosphere and normalized to -1 W m^{-2} (see supplementary Notes 2, supplementary Table 1 and Supplementary Fig. 2 for non-normalized results). The comparison with SO₂ injections clearly shows that, in order to offset the same amount of RF at ToA, using solids as injection material can result in reduced burden (Fig. 1b), stratospheric warming (c) and diffuse radiation (d). Per RF, solids might even treat ozone better, but the uncertainties are currently still prohibitive (e). However, these advantages come at a price: the solids require a higher mass injection rate (a) when injected at 240 nm radius, which would drive up the deployment costs. Yet, considering how high the cost of climate change³⁸ will be in itself, these 50% higher deployment costs might be tolerable given that some environmental risks can be reduced compared to using SO₂.

In the case of SO₂ injections, more than half of the resulting aerosol burden does not need to be lifted to the stratosphere, but is formed in-situ during S(IV) → S(VI) oxidation and water uptake in the stratosphere. This is partly the reason for the higher injection rates required for calcite and alumina particles compared to injection of SO₂. The stratospheric residence times for the particles in the different scenarios are 0.76, 0.86, and 0.97 years for alumina, H₂SO₄ – H₂O and calcite particles, respectively under 2020 conditions. The residence time is dependent on gravitational settling velocities, which is a function of the particle densities (i.e., 3.95 g/cm³, 1.6 g/cm³, and 2.71 g/cm³, respectively) and the particle radius, which is 240 nm for the solids, whereas the sulfuric acid aerosol have a effective radius of about 300 nm globally averaged at 50 hPa. Additionally, less self-lofting of solid particles due to reduced stratospheric heating¹⁶ contributes to a better injection efficiency per unit of RF for SO₂ compared to calcite and alumina particles. The injection rates of sulfur species per RF could be further lowered by a factor of two if elemental sulfur could be injected and oxidized in-situ immediately after release³⁹. However, other solid materials with better scattering properties injected at smaller radius such as diamond particles at 160 nm radius, were shown to require substantially smaller injection rates per RF compared to injecting SO₂^{22,40}. The injection efficiency per RF of calcite and alumina particles could also be increased by extending the stratospheric residence time of the particles through injection of particles smaller than 240 nm instead^{22,34}. However, using smaller particles would also lead to more efficient agglomeration through coagulation, which in turn reduces the backward to forward scattering ratio of visible light^{22,34}. Moreover, smaller injected particle radii provide greater surface area densities (SAD) for heterogeneous reactions that damage the global ozone layer³³.

The large uncertainties in ozone (dashed bars in Fig. 1e) are due to heterogeneous chemistry on solid particles, which is presently still poorly constrained under conditions of stratospheric trace gas concentrations, temperature and relative humidity^{21,33}. The dashed bars in Fig. 1e represent the highest and lowest conceivable physicochemical sensitivity estimates of stratospheric ozone impacts (see Section Stratospheric ozone chemistry). Solid particle SAI would only lead to reduced disturbance of stratospheric ozone compared to injection of SO₂ if the presently most reasonable estimates of heterogeneous uptake coefficients can be confirmed experimentally (solid bars in Fig. 1e).

Stratospheric warming and dynamical response

The major advantage of SAI using solid particles compared to sulfuric acid aerosols is reduced stratospheric heating due to less longwave absorption of

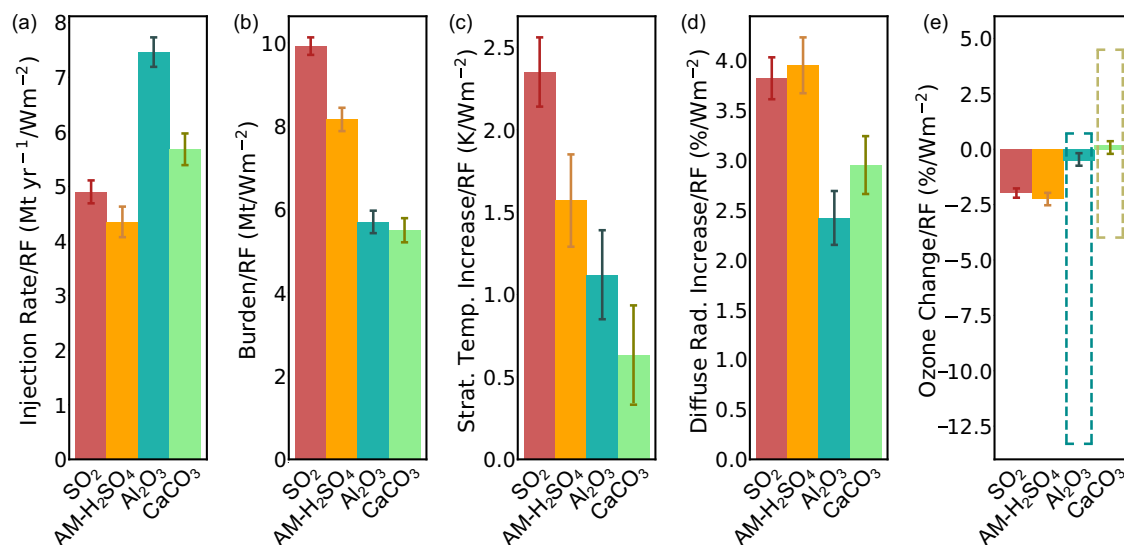


Fig. 1 | Global mean quantities normalized by RF for 2020 conditions. Calculated injection rates and associated side effects to achieve the same global cooling for four different types of materials that could be used in climate intervention via stratospheric aerosol injection. Global means of (a) stratospheric mass injection rate, (b) stratospheric aerosol burden, (c) stratospheric heating at 50 hPa altitude, annually and zonally averaged between 30°N and 30°S, (d) diffuse radiation increase, and (e) change in total ozone column decrease, all normalized to -1 W m^{-2} total all sky ToA RF (see also supplementary Table 1 and Supplementary Fig. 2). Colored bars show mean results for each of the injected materials: red for gaseous SO_2 , orange for accumulation mode sulfuric acid aerosols (AM – H_2SO_4), dark green for alumina

($r = 240 \text{ nm}$), and light green for calcite particles ($r = 240 \text{ nm}$). Uncertainty bars show the standard deviation of inter-annual variability within the 45 years of time slice simulations. For ozone, solid bars show the results for the most reasonable uptake coefficients (see Section Stratospheric ozone chemistry), dashed bars the highest and lowest conceivable physicochemical sensitivity estimates (see Section Stratospheric ozone chemistry). All results refer to conditions of the year 2020 (see Methods). Quantities normalized to resulting stratospheric aerosol burden or injection rate instead of RF are shown in Supplementary Fig. 3 for 2020 conditions, whereas results for 2090 conditions are shown in Supplementary Fig. 4.

alumina and especially calcite particles (Fig. 2a, c). For an injection of 5 Mt yr^{-1} , SOCOL-AERv2 shows a warming of the tropical stratosphere, where most of the aerosol resides, of at most 0.8 K for calcite, but up to 2.5 K for SO_2 . Consequently, the effects of calcite particles on the Brewer-Dobson circulation (BDC) are dwarfed by the impacts of SO_2 injections, where the age of air in the middle stratosphere is up to 3 months younger compared to the calcite experiment or the 2020 reference experiment (Fig. 2b). This indicates a faster overturning, and enhanced mixing of tropical and extratropical stratospheric air masses which is in agreement with findings of previous studies³⁰. Increased tropical stratospheric heating has also been shown to have major implications for the stratosphere-troposphere coupling and tropospheric circulation^{11,31,41}.

According to our model calculations, the aerosol heating would also lead to a warming of the tropical cold point tropopause, which would lead to an increase in stratospheric humidity⁴². Since H_2O is an important GHG, increasing stratospheric H_2O mixing ratios would not only alter stratospheric chemistry and composition via an enhanced stratospheric HO_x ozone depletion cycle, but also alter the radiative balance of the stratosphere and troposphere, inducing a positive RF⁴¹. For injections of 5 Mt yr^{-1} , we found an increase in H_2O of 0.75 ppm ($+18.0\%$) in the lower stratosphere for SO_2 . Most remarkably, alumina and calcite injections lead to a much smaller H_2O increase of less than 0.12 ppm and 0.10 ppm , respectively ($+3\%$ and $+2.5\%$, Supplementary Fig. 5).

Independent of the injected material, the effects of SAI also depend on the background conditions, which are largely influenced by anthropogenic forcings like GHG and ODS emissions; for example, changes in the general circulation can alter aerosol transport patterns⁴³. This effect becomes clear when comparing age of air (AoA) of the 2090 reference simulation to the 2020 reference simulation, which decreases by about 20–30% (not shown). The decrease in AoA is the result of a faster BDC, stronger and more efficient mixing across latitudes⁴⁴ as well as faster exchange between troposphere and stratosphere⁴⁵ in a future warmer climate. The faster BDC effectively decreases the stratospheric residence time of the particles. Therefore, the

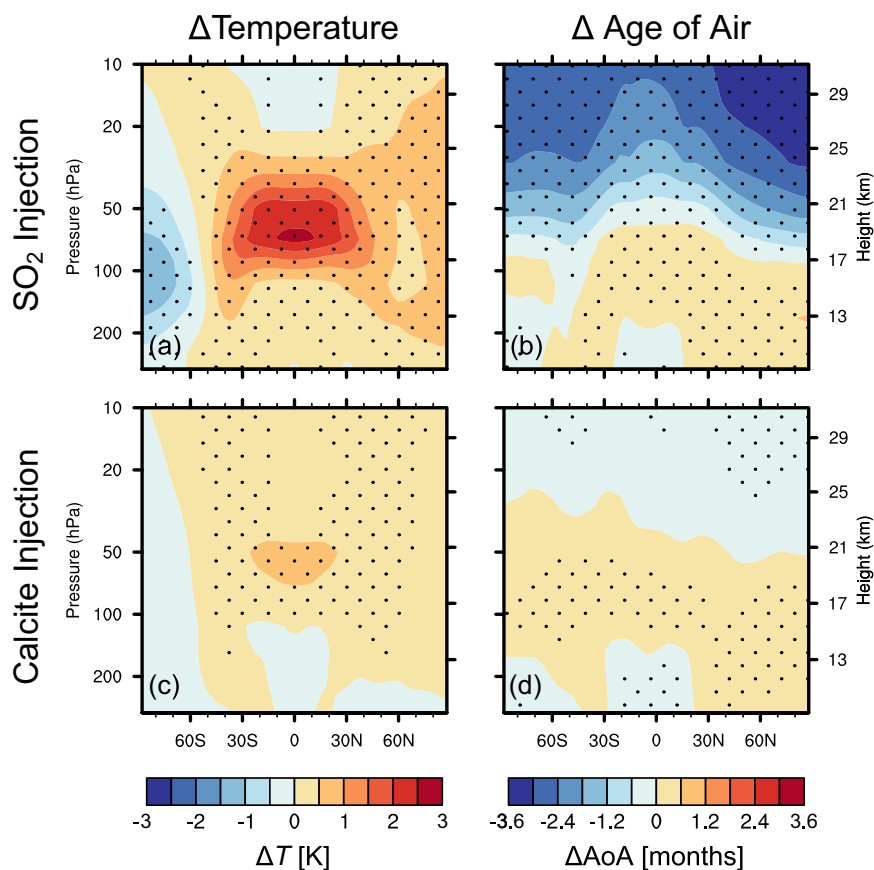
same scenarios under 2090 conditions result in 5–20% smaller aerosol burdens (supplementary Table 1) compared to 2020 conditions.

Impacts on potential ecological drivers

Besides the effects associated with reduced tropospheric temperatures, potential ecological impacts from SAI can arise, among others, from changes in air humidity, increased UV irradiation, increased diffuse radiation and changes in precipitation patterns⁴⁶. Changes in diffuse radiation, as manifested in the whitening of the skies⁴⁷, can considerably affect ecosystems, crop yields and the net primary production rates^{23,48–50}, although the effects depend on the specific plant species and ecosystem under consideration, and model formulation. While current studies generally suggest increases in plant productivity from increased diffuse radiation, capping changes in diffuse radiation would reduce the risk of unforeseen impacts of SAI on ecosystems. The increase in diffuse radiation is determined by particle size, refractive index and stratospheric burden. The former two are larger for solid particles than for $\text{H}_2\text{SO}_4 - \text{H}_2\text{O}$, but the burden, whose influence dominates, is nearly halved. This leads to less diffuse radiation from solid particle SAI when normalized to the resulting RF, namely less than $6\%/(\text{W m}^{-2})$, compared to up to $10\%/(\text{W m}^{-2})$ for sulfur-based SAI (see Figs. 1d and 3a, c).

One matter of concern might be the interaction with ecosystems via deposition of solid particles at the surface. We argue that the ecological impacts of alumina and calcite deposition are expected to be small, since both materials are naturally abundant and natural dust emissions by orders of magnitude larger⁵¹. Similar to SO_2 injections, the deposition patterns of solid particles when injected into the stratosphere will be different compared to natural dust injections into the troposphere (Fig. 3b, d)⁵². The calcite and alumina particle deposition fluxes follow the pattern of global precipitation patterns since more than 98% of the injected alumina and calcite particles are deposited via wet deposition (Fig. 3d). Near-ground concentrations of these particles are, thus, negligible (about $10^{-8} \mu\text{g}/\text{m}^3$) compared to the $\text{PM}_{2.5}$ concentrations, especially in the densely populated regions⁵³, but the

Fig. 2 | Changes in stratospheric temperature and age of air caused by SO₂ or calcite injections for 2020 boundary conditions. Left column: zonally averaged temperature anomaly compared to the reference run for SO₂ (top row) or calcite (bottom row). Right column: corresponding anomaly of the age of air (AoA) in months. Dotted area: statistically significant within the 95% confidence interval (*t*-test). See Supplementary Fig. 5 for zonal mean wind, H₂O and ozone anomalies for 2020 GHG and ODS conditions and Supplementary Fig. 6 for 2090 conditions.



ecological impact of seeding the deposition regions with these materials must still be carefully assessed.

Stratospheric ozone chemistry

An important measure of the environmental side effects of SAI is the ozone column. Changes in ozone have first-order impacts on UV exposure, especially over populated areas like tropics and sub-tropics, and are thus of great societal relevance. Past studies used a large set of assumptions concerning the chemical impacts of solid particles on ozone^{15,35}. Further, they did not attempt to quantify the uncertainty arising from the existing spread in laboratory data. This particularly concerns the efficiency of the uptake of stratospheric acids on the solid particles surface. We provide explicit calculations of the ozone changes arising from such process uncertainty, as discussed next. Using the most reasonable estimates from current knowledge of heterogeneous chemistry on alumina and calcite particles, we simulate a smaller ozone column change compared to the sulfur-based scenarios (thick lines in Fig. 4). The key here is the large uncertainty arising from different assumptions in heterogeneous chemistry, which is highlighted by the shaded areas. The impact on stratospheric chemistry and related uncertainties would decrease sizably compared to present-day conditions, if SAI was done in the future (2090), due to decreasing stratospheric chlorine loading (Fig. 4b).

Since the interactions of calcite and alumina with stratospheric acids (i.e., HCl, HNO₃, and H₂SO_{4(aq)}) at stratospheric temperatures (< 220 K), relative humidity (< 5%) and strong UV irradiation are so poorly known, we ran three simulations for each injection scenario (alumina, calcite and SO₂), namely for the most reasonable interaction (solid bars in Fig. 1 and thick lines in Fig. 4), as well as for the upper and lower limit estimates of effects on the ozone column (dashed bars in Fig. 1 and thin lines in Fig. 4).

For the injection of alumina particles, we extrapolate the measured uptake coefficients of ClONO₂ in Reaction (2)⁵⁴ to stratospheric partial pressures of HCl by using a Langmuir-Hinshelwood molecular

description of co-adsorption/desorption and reaction³³. The maximum ozone loss predicted by the model comes from simulations, in which we assume that HCl does not dissociate, resulting in $\gamma_{\text{ClONO}_2} = 0.019$ under stratospheric conditions. This assumption would cause a sizable globally averaged ozone column destruction of 9.1% for 5 Mt yr⁻¹ injection of calcite particles or 14% per unit of RF. This is about double the historical peak ozone depletion recorded in the 90s due to emissions of ODS¹⁰. However, this is inherently uncertain as it is unclear to what extent HCl dissociates at the surface, and furthermore there are no measurements that account for the potential co-adsorption and dissociation of HNO₃. The latter would likely decrease the surface coverage of HCl substantially³³ and thus, lower the heterogeneous reaction rate of Reaction (2) and ozone depletion (Fig. 4).

For the injection of calcite particles, the uptake of HNO₃ and HCl is limited by $\gamma \lesssim 10^{-3}$, because multiple monolayers of Ca(NO₃)₂ and CaCl₂ are formed within a day, which increase the diffusion impedance for Reactions (4) and (3)³⁷ (see supplementary Notes 3 and supplementary Table 2). Therefore, we performed a simulation with $\gamma_{\text{HCl}} = 10^{-5}$ and $\gamma_{\text{HNO}_3} = 10^{-3}$, which represents a lower limit for the ozone column with a mean global depletion of 3.9%, a possible scenario not considered in previous studies. The ozone loss is due to the removal of NO_x from the stratosphere and thus a lower availability of NO₂ for the deactivation of ClO_x via $\text{NO}_2 + \text{ClO} + \text{M} \rightarrow \text{ClONO}_2 + \text{M}$. Conversely, $\gamma_{\text{HCl}} = 10^{-3}$ and $\gamma_{\text{HNO}_3} = 10^{-5}$ represent an upper limit that leads to a recovery of the ozone hole^{21,35}. Most strikingly, using these values leads to removal of chlorine from the stratosphere, resulting in an increase in the annually averaged ozone column of up to 25% in the south polar region when injecting 5 Mt yr⁻¹ and 4% globally per unit of global RF. However, same as in the case of alumina injections, the assumptions of the extreme scenarios are less likely, as the uptake of HNO₃ and HCl on calcite decreases significantly with time due to the sealing of the surface (whereas we assume that γ_{HCl} and γ_{HNO_3} remain

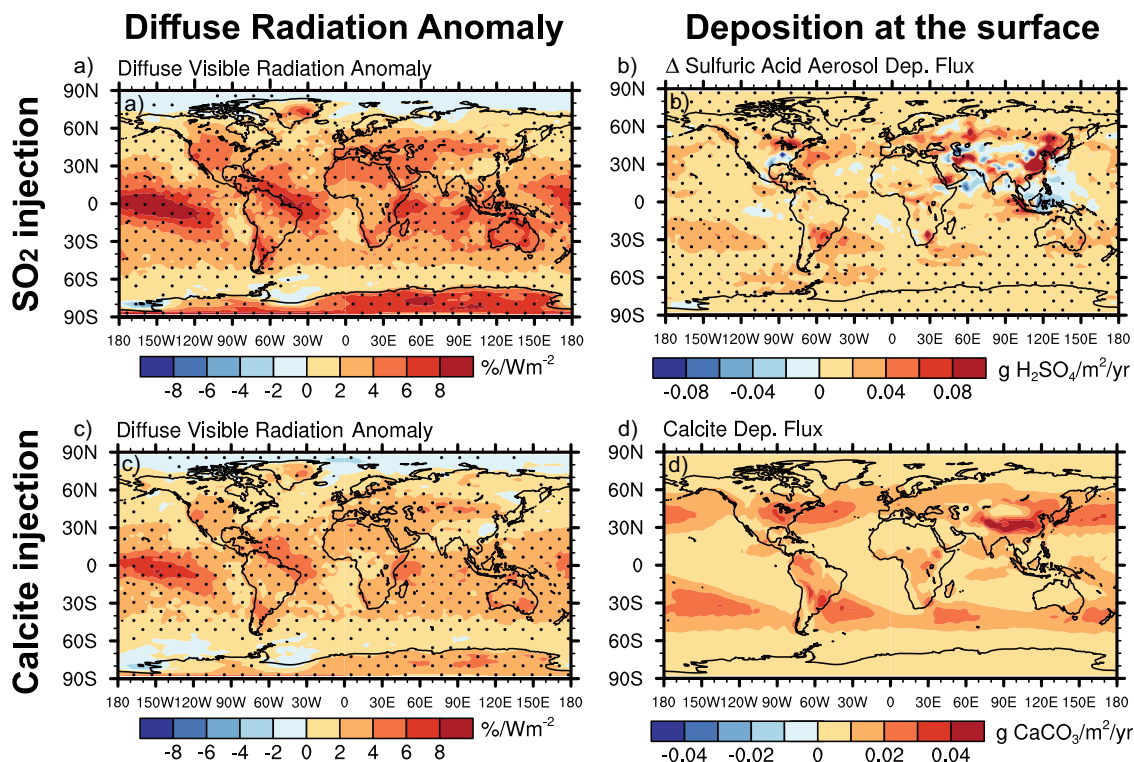


Fig. 3 | Impacts on ecosystems through diffuse radiation and deposition changes of different SAI materials. Left column: changes in diffuse radiation (ultraviolet and visible, 250 nm–680 nm) normalized to ToA total sky RF for SO₂ (a) and calcite (c) injection scenarios. Right column: the anomaly of the total sulfur-equivalent H₂SO₄ deposition flux of the SO₂ injection scenario compared to the reference scenario (b) as well as the total deposition fluxes (sum of wet and dry deposition) of calcite

particles at the surface (d). Dotted areas: statistically significant data in the 95% confidence interval (Student's test), except for the deposition of calcite particles, for which no significance can be calculated. The scenarios with AM – H₂SO₄ and alumina injections (not shown) lead to similar deposition and scattered radiation patterns as SO₂ and calcite, respectively.

constant). Furthermore, the uptake of the two acids is likely to be similar and the effects on ozone would cancel each other out.

For SO₂ injections, lower and upper bounds for the ozone column response were estimated by multiplying or dividing the heterogeneous reaction rate of N₂O₅ hydrolysis (Reaction (1)) by a factor of 2 and heterogeneous reactions of chlorine and bromine activation by a factor of 5, based on uncertainty estimates of measured reaction rates at stratospheric temperatures and trace gas concentrations^{36,55}.

In passing we note that the uncertainty ranges given for the injection of solid particles are based only on Reaction (1) for aluminum oxide and Reactions (3) and (4) for calcite. No experimental data are available for other reactions on these particle types. In addition, since calcite ages chemically in the stratosphere, the largest uncertainties result from changes in surface properties over time⁵⁶. CaSO₄, CaCl₂ and Ca(NO₃)₂ as well as their hydrates could harbor different heterogeneous reactions with different reaction rates compared to calcite particles, whereby the heterogeneous chemistry on the calcite particles changes over time as a function of chemical aging. In addition, the heterogeneous chemistry depends on the available SAD and, thus, on particle size. Injecting smaller particles would sizably enhance the resulting effects on the ozone column, as we have recently shown³³.

Changes in stratospheric ozone concentrations may also impact stratospheric temperatures and thus the circulation response and resulting RFs. The alumina injection scenario in which HCl does not dissociate (Fig. 1e) shows sizable ozone changes in the lower stratosphere, and a global ozone column depletion of 14%/Wm⁻². These ozone changes would cool the lower stratosphere by 1.9 K/Wm⁻², completely offsetting the warming of the alumina particles (Fig. 1c). This highlights the importance of interactively

coupling heterogeneous chemistry with radiative effects of the solid particles when modeling the SAI response on climate.

Discussion

For the assessment of the risks and benefits of SAI of solid particles it is crucial to employ models with sufficient complexity informed by experimental data and interactivity between the essential model components, which was a limitation in previous studies^{15,19,35}. This was achieved for the first time in this study by using an interactive ACCM incorporating a solid particle microphysics scheme³⁴. We show that the main advantage of SAI by alumina and especially calcite particles is the sizably reduced heating of the stratosphere. This leads to much smaller stratospheric changes, such as acceleration of the BDC, of zonal winds or increasing stratospheric humidity (Supplementary Figs. 6 and 7), which could have important implications for the tropospheric circulation and regional climate^{11–13}. It has been shown for SO₂ injections that such dynamical side effects could be reduced by using more complex injection strategies^{31,57}, while in our study we only considered tropical injections. Furthermore, the side effects on tropospheric climate and ecosystems are potentially reduced when using solid particles, as they induce smaller changes in diffuse radiation, ozone depletion and UV enhancement compared to SO₂ injections, albeit with greater uncertainties.

Even though there is evidence that particle aging processes do not sizably affect the scattering properties of solid particles³⁴, this is another factor which might introduce uncertainty to our results which requires further research. Despite the larger scattering cross sections of alumina and calcite particles compared to sulfuric acid, they require higher mass injection rates to achieve the same RF (see the overview provided in Fig. 5). This is primarily due to the in-situ oxidation of SO₂, which results in the biggest part of sulfuric acid aerosol burden already being in the stratosphere. Under

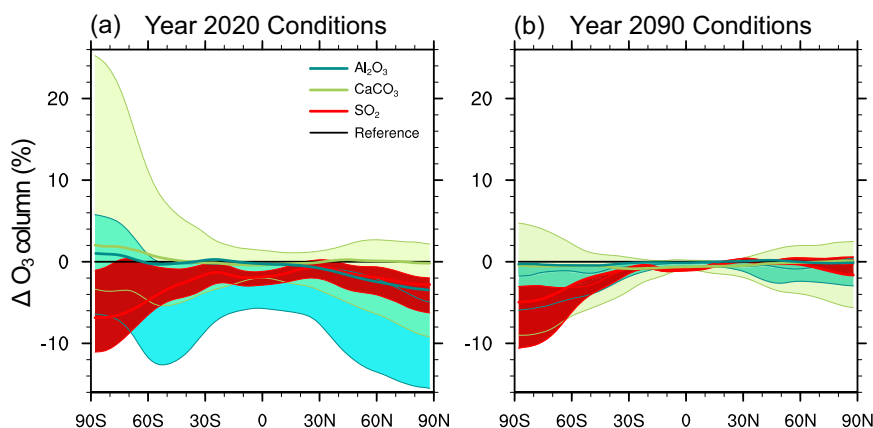


Fig. 4 | Zonally averaged ozone column changes and related uncertainties for injections of 5 Mt of material per year. Injections of SO_2 are shown in red, alumina ($r = 240$ nm) in blue and calcite ($r = 240$ nm) in green. Thick lines: most reasonable uptake coefficients (Section SAI microphysics and heterogeneous chemistry). Shaded areas show corresponding uncertainties (see Methods): in blue for alumina assuming full coverage by $\text{H}_2\text{SO}_4 - \text{H}_2\text{O}$ for the upper and non-dissociative HCl uptake without $\text{H}_2\text{SO}_4/\text{HNO}_3$ co-adsorption for the lower limit³³; in green for calcite

assuming $\gamma_{\text{HCl}} = 10^{-3}$ and $\gamma_{\text{HNO}_3} = 10^{-5}$ for the upper and $\gamma_{\text{HCl}} = 10^{-5}$ and $\gamma_{\text{HNO}_3} = 10^{-3}$ for the lower limit; in red for SO_2 assuming heterogeneous reaction rate coefficients to be higher or lower than recommended values⁵⁶ by a factor of 2 for Reaction (1) and by a factor of 5 for the heterogeneous chlorine and bromine activation reactions. **a** For 2020 and **(b)** for 2090 boundary conditions. For underlying SADs see Supplementary Fig. 7.

conditions for the year 2090 and assuming a high GHG emissions scenario, even larger alumina and calcite particle injections would be required to achieve the same cooling of -1 W m^{-2} compared to 2020 conditions (see Fig. 5). This might be related to various effects such as warmer surface temperatures, a faster BDC and larger water vapor concentrations in a future warmer climate. This is not as pronounced in the SO_2 injection case which points to non-linearity in the response to different materials, which merits further investigation.

Our model calculations with alumina and calcite SAI, when performed on the basis of the current knowledge with the most reasonable assumptions for heterogeneous reaction rates on these materials, exhibit lower ozone depletion rates compared to sulfur-based scenarios. However, due to very limited experimental data on heterogeneous chemistry on solid particles under stratospheric conditions, the modeled ozone response is largely dependent on the underlying assumptions. Therefore, the uncertainties regarding the modeled ozone are considerable, so that both sizable ozone depletion or, in the case of calcite particles, an increase in ozone cannot be entirely ruled out (see Fig. 5). While the impact of sulfur-based SAI on stratospheric chemistry appears to be subject to less uncertainty and therefore be considered potentially safer, SAI via solid particles has potential for substantially reduced side effects in the Earth System. Their greater uncertainties can only be reduced by concerted laboratory efforts.

In addition to the so far discussed risks and benefits of SAI by solid particles, there are a number of other unresolved challenges. First, it is subject to uncertainty that mono-disperse solids can be dispersed into the stratosphere from aircraft in large enough quantities to compete with the relatively simple and fast release of gaseous SO_2 ⁵⁸. Second, modeled injections were continuous over time and equally distributed into the grid boxes of SOCOL-AERv2 which has a horizontal resolution of $325 \text{ km} \times 325 \text{ km} \times 1.5 \text{ km}$ at 50 hPa in the equatorial stratosphere, thereby neglecting sub-model-grid-scale microphysical processes occurring within the injection plume of an aircraft. It has been shown that agglomeration could significantly decrease the scattering efficiency of solids²². Third, aerosol-cloud interaction are still highly uncertain and could substantially alter the resulting RF. Calcite particles for example were shown to be good ice nucleation particles, which could increase cirrus cloud coverage and thus weaken the RF from calcite particles⁵⁶. However, same as for sulfur-based SAI, the cirrus cloud effect of SAI remains subject to large process uncertainty and requires further research.

It is important to highlight that SAI is not a substitute for climate mitigation technologies, which tackle the root cause of climate change,

such as getting to global net-zero GHG emissions and scaling up GHG removal methods. Rather, SAI would represent a temporary measure, which could help shaving the peak of global warming and avoid reaching climate tipping points. To inform potential future decision-makers about risks and benefits of SAI, it is important to thoroughly study the associated physical, ethical and social impacts and uncertainties. With our study we show that consideration of SAI of solid particles as an alternative to sulfuric acid particles requires coordinated, collaborative laboratory research to investigate their detailed optical properties as a function of aging in the stratosphere, their ice nucleation properties as well as the heterogeneous chemistry on solid particles at stratospheric temperatures, partial pressures of relevant trace gases, relative humidity and stratospheric UV irradiation. High-quality laboratory data in combination with Earth System modeling would constrain the process uncertainties of SAI of solid particles. Given the large potential of reducing undesirable side-effects on the global environment of this climate intervention strategy, we encourage conducting this research.

Methods

The interactive solid particle microphysics scheme in SOCOL-AERv2

We use the ACCM SOCOL-AERv2⁷, which is based on ECHAM5.4 general circulation model⁵⁹, coupled to the chemistry module MEZON⁶⁰ and the aerosol microphysics module AER^{61,62}. SOCOL-AERv2 features a vertical resolution of 39 sigma-pressure levels, extending up to 0.01 hPa (about 80 km altitude), with a horizontal resolution of T42 ($2.8^\circ \times 2.8^\circ$). Dynamics are updated every 15 min, while chemistry calculations occur every 2 h with a 2 min subimestep for microphysics. Treatment of sulfuric acid aerosols in the model and their various effects have been extensively validated against observations and other models for volcanic cases^{63,64}, background aerosol layer^{7,65}, and sulfur-based SAI^{11,32,66,67}. A detailed description of the solid particle microphysics module incorporated in SOCOL-AERv2 is available in a previous publication³⁴. The model simulates the injection and advection of solid particles and their microphysical interactions such as settling, agglomeration via self-coagulation, coagulation with sulfuric acid aerosols, condensation of H_2SO_4 on the particle surface and the settling of the solid particles interactively coupled to the model's radiation and heterogeneous chemistry schemes³⁴. The model allows for representation of heterogeneous chemistry on the solid particles³³. The solid particles are also coupled to the model's long- and shortwave radiation code via their scattering and absorption cross sections³⁴.

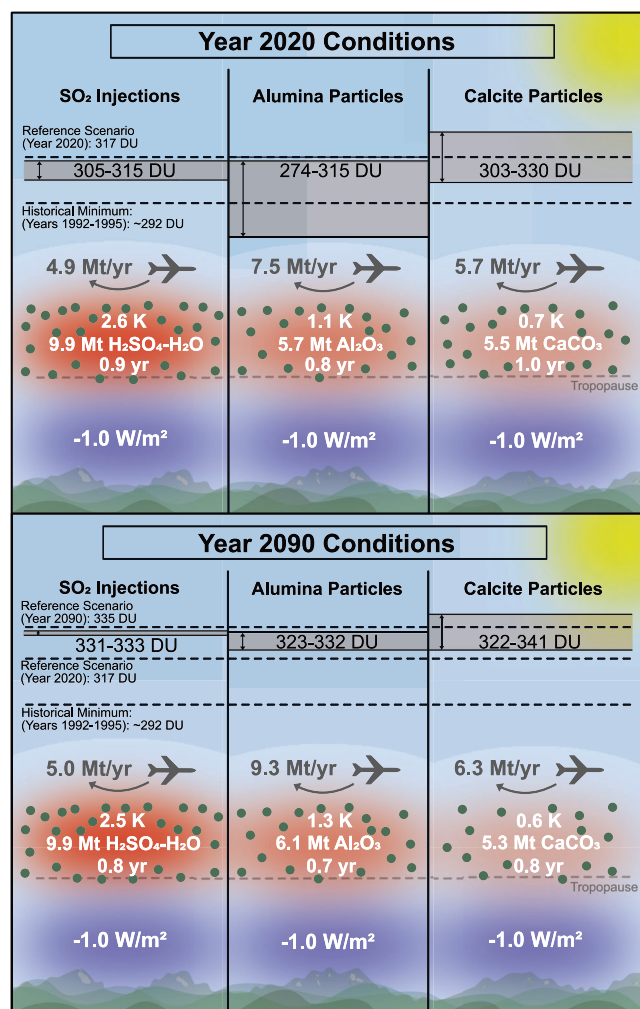


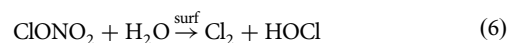
Fig. 5 | Schematic overview of globally averaged quantities linearly normalized from 5 Mt yr⁻¹ injections to -1 W m⁻² total all sky ToA RF. Upper part shows results for 2020 and lower part for 2090 boundary conditions in respect to GHG, sea surface temperatures (SST), sea ice concentrations (SIC) and ODS concentrations when injecting gaseous SO₂ (left), alumina (middle) and calcite (right) particles at radius of 240 nm. Shown are required stratospheric aerosol burden in Mt, the injection rate in Mt yr⁻¹, the resulting global average stratospheric residence time of the particles in years, the resulting heating in the tropical stratosphere in K and the resulting ozone column in Dobson units (DU). For comparison the ozone column of the reference scenario, the historical minimum in the years 1992–1995 (modeled by SOCOL-AERv2) as well as the uncertainty ranges for the resulting ozone column (grey areas) are shown (see Section Stratospheric ozone chemistry for details on the uncertainty ranges). For 2090 conditions also the 2090 reference ozone column is shown.

We focus on alumina and calcite particle injection since these are the only potential injection candidates for which some experimental data on heterogeneous chemistry in the stratosphere is available^{21,54,68,69}. The model treats alumina and calcite particles as very different representatives of solid particles concerning their interaction with stratospheric chemistry.

On the one hand, alumina is thought to be largely unreactive and the bulk of the particles (i.e., Al₂O₃) will most likely not undergo chemical reactions in the stratosphere³³, whereas calcite is a base and is thus expected to readily react with most of the acidic molecules available in stratospheric air (i.e., mainly HNO₃, HCl, and H₂SO₄). However, alumina particles still provide surfaces, which allow for adsorption of HCl and HNO₃ as well as for the uptake of H₂SO₄. Thus, the solid particle microphysics model takes into account coagulation of solid particles with H₂SO₄ - H₂O aerosols as well as condensation of gaseous H₂SO₄ on alumina surfaces. The condensed

H₂SO₄ - H₂O is represented on the alumina particles assuming a contact angle of H₂SO₄ - H₂O on alumina particles of about 30°^{33,34}. This leaves parts of the alumina surface uncovered and available for hosting, for example, the heterogeneous reaction HCl + ClONO₂ → Cl₂ + HNO₃, whose rate constant on alumina surfaces has been measured in a study which explored chlorine activation on alumina containing space shuttle exhaust⁵⁴.

For heterogeneous chemistry on alumina particles, we accounted for Reaction (2) by applying a Langmuir-Hinshelwood description of adsorption and reaction for the uptake coefficient of ClONO₂. Experimentally measured uptake coefficients of ClONO₂⁵⁴ were extrapolated to stratospheric partial pressures by using the “dissociative HCl” parameterisation derived in a previous study³³ and assuming co-adsorption of HNO₃. Additionally, for Reactions (1), (6), and (7) we applied the same heterogeneous reaction rates as for sulfuric acid aerosols (Section SAI microphysics and heterogeneous chemistry).



On the other hand, calcite particles are thought to react with HNO₃, HCl, and H₂SO₄ thereby potentially altering the composition of the particles. Therefore, calcite is an example of a material which is expected to undergo chemical aging in the stratosphere, thereby altering its chemical and optical properties over the course of its stratospheric residence time. In case of SAI of calcite, the model thus allows for particle composition changes via uptake of HNO₃, HCl, and H₂SO₄ resulting in particle mixtures of CaCO₃, CaSO₄, Ca(NO₃)₂ and CaCl₂³⁴.

For heterogeneous chemistry on calcite particles we followed previous studies^{21,37} and applied uptake coefficients of 10⁻⁴ for HNO₃, 10⁻⁵ for HCl on timescales relevant for the stratosphere, even though other studies have measured much larger initial uptake coefficients^{68,69}. However, these uptake coefficients cannot be maintained for relevant timescales due to increased passivation of the surface with reaction products with time³⁷. Conversely, the uptake coefficient for H₂SO₄ was kept at 1.0 for all calcite simulations, since H₂SO₄ has a very low equilibrium vapor pressure.

Experimental setup

Each perturbation experiment injected 5 Mt of material per year at 50 hPa (~20 km altitude) equally distributed in all model grid cells between 30°N and 30°S at all longitudes with particle radii of 240 nm for alumina and calcite injections, which are the baseline simulations performed in a previous study³⁴. These simulations were extended to 45 years to get a more robust estimate of the effective RF. Each simulation spanned over 50 years, of which the first 5 years served as spin-up to equilibrate stratospheric aerosol burdens. Thus, a total of 5 simulations for the reference run and four perturbation experiments with injections of 5 Mt yr⁻¹, Al₂O₃, CaCO₃, SO₂ and direct injections of accumulation mode sulfuric acid aerosols (AM - H₂SO₄, i.e., log-normally distributed with $r_m = 0.095 \mu\text{m}$ and $\sigma = 1.5$). The latter scenario assumes that an optimized aerosol size distribution with a mode radius of 0.095 μm can be produced by injecting gaseous H₂SO₄ into an aircraft plume^{32,66,70,71}. We assumed injection rates of absolute masses and not sulfur equivalent masses since injection of elemental sulfur might not be technically feasible³⁹. In addition to the baseline experiments with timeslice boundary conditions with climatological SST, and SIC, GHG, and ODS concentrations set to year 2020 the five ensembles were also simulated for timeslice 2090 boundary conditions. GHG and ODS concentrations were taken from SSP5-8.5⁷² and⁷³, respectively, while SST and SIC were taken from a 10-year average (2011–2020) of the Hadley dataset⁷⁴ for 2020 conditions and from the RCP8.5 scenario (2090–2099) simulated by CESM5-CAM1 for 2090 conditions⁷⁵. Since we are using fixed SST and SIC, it is not possible to calculate the surface cooling effect. We refrain from inferring the potential surface cooling effect by using available estimates of climate sensitivity (quantified as units of surface temperature

change per unit of RF from CO₂) since the efficacy of SAI as a climate driver might be different from that of CO₂ and other GHGs. SAI and GHGs as a climate driver scatter and absorb in very different wavelengths, respectively and the associated climate feedbacks are likely also different.

Data availability

The data is available on an online repository (<https://doi.org/10.3929/ethz-b-000670453>)⁷⁶.

Code availability

The model code is available on an online repository (<https://doi.org/10.5281/zenodo.8398627>)⁷⁷ or on request from the corresponding author.

Received: 24 September 2024; Accepted: 15 January 2025;

Published online: 21 February 2025

References

- Budyko, M. *Climatic Changes*, Vol. 10 (American Geophysical Union, Washington, DC, 1977).
- Crutzen, P. Albedo enhancement by stratospheric sulfur injections: a contribution to resolve a policy dilemma? *Clim. Change* **77**, 211–220 (2006).
- Keith, D. W. & MacMartin, D. G. A temporary, moderate and responsive scenario for solar geoengineering. *Nature Clim. Change* **5**, 201–206 (2015).
- MacMartin, D. G., Ricke, K. L. & Keith, D. W. Solar geoengineering as part of an overall strategy for meeting the 1.5°C Paris target. *Philos. Trans. R. Soc. A: Math., Phys. Eng. Sci.* **376**, 20160454 (2018).
- Mills, M. J. et al. Global volcanic aerosol properties derived from emissions, 1990–2014, using cesm1(waccm). *J. Geophys. Res.: Atmos.* **121**, 2332–2348 (2016).
- Sukhodolov, T. et al. Stratospheric aerosol evolution after Pinatubo simulated with a coupled size-resolved aerosol-chemistry-climate model, SOCOL-AERv1.0. *Geosci. Model Dev.* **11**, 2633–2647 (2018).
- Feinberg, A. et al. Improved tropospheric and stratospheric sulfur cycle in the aerosol-chemistry-climate model SOCOL-AERv2. *Geosci. Model Dev.* **12**, 3863–3887 (2019).
- Timmreck, C. et al. The interactive stratospheric aerosol model intercomparison project (ISA-MIP): motivation and experimental design. *Geosci. Model Dev.* **11**, 2581–2608 (2018).
- Quaglia, I. et al. Interactive stratospheric aerosol models' response to different amounts and altitudes of SO₂ injection during the 1991 pinatubo eruption. *Atmos. Chem. Phys.* **23**, 921–948 (2023).
- WMO. Scientific assessment of ozone depletion: 2022. *Glob. Ozone Res. Monit. Proj., World Meteorol. Organ.* **278**, 509 (2022).
- Wunderlin, E. et al. Side effects of sulfur-based geoengineering due to absorptivity of sulfate aerosols. *Geophys. Res. Lett.* **51**, e2023GL107285 (2024).
- Banerjee, A. et al. Robust winter warming over Eurasia under stratospheric sulfate geoengineering – the role of stratospheric dynamics. *Atmos. Chem. Phys.* **21**, 6985–6997 (2021).
- Simpson, I. R. et al. The regional hydroclimate response to stratospheric sulfate geoengineering and the role of stratospheric heating. *J. Geophys. Res.: Atmos.* **124**, 12587–12616 (2019).
- Niemeier, U., Schmidt, H., Alterskjær, K. & Kristjánsson, J. E. Solar irradiance reduction via climate engineering: impact of different techniques on the energy balance and the hydrological cycle. *J. Geophys. Res. Atmos.* **118**, 905–11 (2013).
- Weisenstein, D. K., Keith, D. W. & Dykema, J. A. Solar geoengineering using solid aerosol in the stratosphere. *Atmos. Chem. Phys.* **15**, 11835–11859 (2015).
- Haywood, J. M., Jones, A., Johnson, B. T. & McFarlane Smith, W. Assessing the consequences of including aerosol absorption in potential stratospheric aerosol injection climate intervention strategies. *Atmos. Chem. Phys.* **22**, 6135–6150 (2022).
- Ferraro, A. J., Highwood, E. J. & Charlton-Perez, A. J. Stratospheric heating by potential geoengineering aerosols. *Geophys. Res. Lett.* **38**, L24706 (2011).
- Ferraro, A. J., Charlton-Perez, A. J. & Highwood, E. J. Stratospheric dynamics and midlatitude jets under geoengineering with space mirrors and sulfate and titania aerosols. *J. Geophys. Res.: Atmos.* **120**, 414–429 (2015).
- Dykema, J. A., Keith, D. W. & Keutsch, F. N. Improved aerosol radiative properties as a foundation for solar geoengineering risk assessment. *Geophys. Res. Lett.* **43**, 7758–7766 (2016).
- Jones, A. C., Haywood, J. M. & Jones, A. Climatic impacts of stratospheric geoengineering with sulfate, black carbon and titania injection. *Atmos. Chem. Phys.* **16**, 2843–2862 (2016).
- Dai, Z., Weisenstein, D. K., Keutsch, F. N. & Keith, D. W. Experimental reaction rates constrain estimates of ozone response to calcium carbonate geoengineering. *Commun. Earth Environ.* **1**, 63 (2020).
- Vattioni, S. et al. Microphysical interactions determine the effectiveness of solar radiation modification via stratospheric solid particle injection. *Geophys. Res. Lett.* **51**, e2024GL110575 (2024).
- Xia, L., Robock, A., Tilmes, S. & Neely, R. R. Stratospheric sulfate geoengineering could enhance the terrestrial photosynthesis rate. *Atmos. Chem. Phys.* **16**, 1479–1489 (2016).
- Zarnetske, P. L. et al. Potential ecological impacts of climate intervention by reflecting sunlight to cool Earth. *Proc. Natl. Acad. Sci. USA* **118**, e1921854118 (2021).
- Aquila, V., Garfinkel, C. I., Newman, P., Oman, L. & Waugh, D. Modifications of the quasi-biennial oscillation by a geoengineering perturbation of the stratospheric aerosol layer. *Geophys. Res. Lett.* **41**, 1738–1744 (2014).
- Richter, J. H. et al. Stratospheric dynamical response and ozone feedbacks in the presence of SO₂ injections. *J. Geophys. Res.: Atmos.* **122**, 557–12 (2017).
- Jones, A. et al. The impact of stratospheric aerosol intervention on the North Atlantic and Quasi-Biennial Oscillations in the Geoengineering Model Intercomparison Project (GeoMIP) G6sulfur experiment. *Atmos. Chem. Phys.* **22**, 2999–3016 (2022).
- Tilmes, S., Müller, R. & Salawitch, R. The sensitivity of polar ozone depletion to proposed geoengineering schemes. *Science* **349**, 1201–1204 (2008).
- Heckendorn, P. et al. The impact of geoengineering aerosols on stratospheric temperature and ozone. *Environ. Res. Lett.* **4**, 045108 (2009).
- Tilmes, S. et al. Stratospheric ozone response to sulfate aerosol and solar dimming climate interventions based on the G6 Geoengineering Model Intercomparison Project (GeoMIP) simulations. *Atmos. Chem. Phys.* **22**, 4557–4579 (2022).
- Bednarz, E. M. et al. Injection strategy – a driver of atmospheric circulation and ozone response to stratospheric aerosol geoengineering. *Atmos. Chem. Phys.* **23**, 13665–13684 (2023).
- Weisenstein, D. K. et al. An interactive stratospheric aerosol model intercomparison of solar geoengineering by stratospheric injection of SO₂ or accumulation-mode sulfuric acid aerosols. *Atmos. Chem. Phys.* **22**, 2955–2973 (2022).
- Vattioni, S. et al. Chemical impact of stratospheric alumina particle injection for solar radiation modification and related uncertainties. *Geophys. Res. Lett.* **50**, e2023GL105889 (2023).
- Vattioni, S. et al. A fully coupled solid-particle microphysics scheme for stratospheric aerosol injections within the aerosol-chemistry-climate model socol-aer2. *Geosci. Model Dev.* **17**, 7767–7793 (2024).
- Keith, D. W., Weisenstein, D. K., Dykema, J. A. & Keutsch, F. N. Stratospheric solar geoengineering without ozone loss. *Proc. Natl. Acad. Sci. USA* **113**, 14910–14914 (2016).
- Burkholder, J. et al. Chemical kinetics and photochemical data for use in atmospheric studies; evaluation number 19. Tech. Rep. 19-5,

- Pasadena, CA: Jet Propulsion Laboratory, National Aeronautics and Space <http://jpldataeval.jpl.nasa.gov> (2020).
37. Vattioni, S. Chemical and climatic impacts of solid particles for stratospheric solar climate intervention. *ETH Zurich Res. Collect.* **29973**, 117–166 (2024).
 38. Newman, R. & Noy, I. The global costs of extreme weather that are attributable to climate change. *Nat. Commun.* **14**, 6103 (2023).
 39. Smith, J. P., Dykema, J. A. & Keith, D. W. Production of Sulfates onboard an aircraft: implications for the cost and feasibility of stratospheric solar geoengineering. *Earth Space Sci.* **5**, 150–162 (2018).
 40. Stefanetti, F. et al. Stratospheric injection of solid particles reduces side effects on circulation and climate compared to SO₂ injections. *Environ. Res.: Clim.* **3**, 045028 (2024).
 41. Banerjee, A. et al. Stratospheric water vapor: an important climate feedback. *Clim. Dyn.* **53**, 1697–1710 (2019).
 42. Dessler, A. E., Schoeberl, M. R., Wang, T., Davis, S. M. & Rosenlof, K. H. Stratospheric water vapor feedback. *Proc. Natl. Acad. Sci.* **110**, 18087–18091 (2013).
 43. Visioni, D. et al. Reduced poleward transport due to stratospheric heating under stratospheric aerosols geoengineering. *Geophys. Res. Lett.* **47**, e2020GL089470 (2020).
 44. Eichinger, R. et al. The influence of mixing on the stratospheric age of air changes in the 21st century. *Atmos. Chem. Phys.* **19**, 921–940 (2019).
 45. Abalos, M. et al. Future trends in stratosphere-to-troposphere transport in ccmi models. *Atmos. Chem. Phys.* **20**, 6883–6901 (2020).
 46. Dagon, K. & Schrag, D. P. Quantifying the effects of solar geoengineering on vegetation. *Clim. Change* **153**, 235–251 (2019).
 47. Kravitz, B., MacMartin, D. G. & Caldeira, K. Geoengineering: whiter skies? *Geophys. Res. Lett.* **39**, L11801 (2012).
 48. Neimane-Šroma, S., Durand, M., Lintunen, A., Aalto, J. & Robson, T. M. Shedding light on the increased carbon uptake by a boreal forest under diffuse solar radiation across multiple scales. *Glob. Change Biol.* **30**, e17275 (2024).
 49. Mercado, L. M. et al. Impact of changes in diffuse radiation on the global land carbon sink. *Nature* **458**, 1014–1017 (2009).
 50. Sonntag, S. et al. Quantifying and comparing effects of climate engineering methods on the earth system. *Earth's Future* **6**, 149–168 (2018).
 51. Laurent, B., Marticorena, B., Bergametti, G., Léon, J. F. & Mahowald, N. M. Modeling mineral dust emissions from the Sahara desert using new surface properties and soil database. *J. Geophys. Res.: Atmos.* **113**, D14218 (2008).
 52. Visioni, D., Pitari, G., Tuccella, P. & Curci, G. Sulfur deposition changes under sulfate geoengineering conditions: quasi-biennial oscillation effects on the transport and lifetime of stratospheric aerosols. *Atmos. Chem. Phys.* **18**, 2787–2808 (2018).
 53. Zhu, Y. & Shi, Y. Spatio-temporal variations of pm2.5 concentrations and related premature deaths in asia, africa, and europe from 2000 to 2018. *Environ. Impact Assess. Rev.* **99**, 107046 (2023).
 54. Molina, M. J., Molina, L. T., Zhang, R., Meads, R. F. & Spencer, D. D. The reaction of clono2 with hcl on aluminum oxide. *Geophys. Res. Lett.* **24**, 1619–1622 (1997).
 55. Ammann, M. et al. Evaluated kinetic and photochemical data for atmospheric chemistry: Volume VI - heterogeneous reactions with liquid substrates. *Atmos. Chem. Phys.* **13**, 8045–8228 (2013).
 56. Cziczo, D. J., Wolf, M. J., Gasparini, B., Münch, S. & Lohmann, U. Unanticipated side effects of stratospheric albedo modification proposals due to aerosol composition and phase. *Sci. Rep.* **9**, 18825 (2019).
 57. Henry, M. et al. Comparison of ukesm1 and cesm2 simulations using the same multi-target stratospheric aerosol injection strategy. *Atmos. Chem. Phys.* **23**, 13369–13385 (2023).
 58. Neukermans, A., Cooper, G., Foster, J., Galbraith, L. & Jain, S. Methods for dispersal of precipitated calcium carbonate for stratospheric aerosol injection. *J. Atmos. Ocean. Technol.* **38**, 1571–1584 (2021).
 59. Roeckner, E. et al. The atmospheric general circulation model ECHAM 5. PART I: Model description. MPI-Report No. 349, Max-Planck-Institut für Meteorologie, Hamburg http://www.mpimet.mpg.de/fileadmin/publikationen/Reports/max_scirep_349.pdf (2003).
 60. Egorova, T., Rozanov, E., Zubov, V. & Karol, I. L. Model for investigating ozone trends (MEZON). *Izvestiya, Atmos. Ocean. Phys.* **39**, 277–292 (2003).
 61. Weisenstein, D. K., Penner, J. E., Herzog, M. & Liu, X. Global 2-D intercomparison of sectional and modal aerosol modules. *Atmos. Chem. Phys.* **7**, 2339–2355 (2007).
 62. Sheng, J. et al. Global atmospheric sulfur budget under volcanically quiescent conditions: aerosol-chemistry-climate model predictions and validation. *J. Geophys. Res. - Atmos.* **120**, 256–276 (2015).
 63. Brodowsky, C. et al. SOCOL-AERv2 model code. *Zenodo* <https://doi.org/10.5281/zenodo.5733121> (2018).
 64. Clyne, M. et al. Model physics and chemistry causing intermodel disagreement within the VoIMIP-Tambora Interactive Stratospheric Aerosol ensemble. *Atmos. Chem. Phys.* **21**, 3317–3343 (2021).
 65. Brodowsky, C. V. et al. Analysis of the global atmospheric background sulfur budget in a multi-model framework. *EGUsphere* **2023**, 1–49 (2023).
 66. Vattioni, S. et al. Exploring accumulation-mode H₂SO₄ versus SO₂ stratospheric sulfate geoengineering in a sectional aerosol-chemistry-climate model. *Atmos. Chem. Phys.* **19**, 4877–4897 (2019).
 67. Vattioni, S. et al. Importance of microphysical settings for climate forcing by stratospheric SO₂ injections as modeled by SOCOL-AERv2. *Geosci. Model Dev.* **17**, 4181–4197 (2024).
 68. Huynh, H. N. & McNeill, V. F. Heterogeneous chemistry of CaCO₃ aerosols with HNO₃ and HCl. *J. Phys. Chem. A* **124**, 3886–3895 (2020).
 69. Huynh, H. N. & McNeill, V. F. Heterogeneous reactivity of HCl on CaCO₃ aerosols at stratospheric temperature. *ACS Earth Space Chem.* **5**, 1896–1901 (2021).
 70. Pierce, J. R., Weisenstein, D. K., Heckendorn, P., Peter, T. & Keith, D. W. Efficient formation of stratospheric aerosol for climate engineering by emission of condensable vapor from aircraft. *Geophys. Res. Lett.* **37**, L18805 (2010).
 71. Benduhn, F., Schallock, J. & Lawrence, M. G. Early growth dynamical implications for the steerability of stratospheric solar radiation management via sulfur aerosol particles. *Geophys. Res. Lett.* **43**, 9956–9963 (2016).
 72. O'Neill, B. et al. The roads ahead: narratives for shared socioeconomic pathways describing world futures in the 21st century. *Global Environ. Change* **42**, 169–180 (2015).
 73. WMO. Scientific assessment of ozone depletion: 2018. *Glob. Ozone Res. Monit. Proj., World Meteorol. Organ.* **50**, 588 (2018).
 74. Kennedy, J. J., Rayner, N., Atkinson, C. & Killick, R. An ensemble data set of sea surface temperature change from 1850: the met office hadley centre hadsst. 4.0.0.0 data set. *J. Geophys. Res.: Atmos.* **124**, 7719–7763 (2019).
 75. Meehl, G. A. et al. Climate change projections in CESM1(CAM5) compared to CCSM4. *J. Clim.* **26**, 6287–6308 (2013).
 76. Vattioni, S. Simulation data for: risks and benefits of stratospheric solar climate intervention via solid particle injections. *ETH Zurich* <https://doi.org/10.3929/ethz-b-000670453> (2024).
 77. Vattioni, S. SOCOL-AER_solid_particles [Software] <https://doi.org/10.5281/zenodo.8398627> (2023b).

Acknowledgements

We especially thank Debra Weisenstein for discussions about her original solid particle AER code as well as David Keith for valuable discussion of our results. We also appreciate Jim Haywood's feedback on the manuscript. Support for Gabriel Chiodo and Andrea Stenke was provided by the Swiss National Science Foundation within the Ambizione grant no. PZ00P2_180043. Gabriel Chiodo also acknowledges funding from the European Commission via the ERC StG 101078127 and the Spanish Ministry of Science and Innovation via the Ramon y Cajal grant (no. RYC2021-033422-I). Support for Sandro Vattioni was provided by the ETH Research grant no. ETH-1719-2 as well as by the Harvard Geoengineering Research Program. Beiping Luo and Sandro Vattioni also acknowledge funding from the Simons Foundation (grant no. SFI-MPS-SRM-00005217). John Andrew Dykema and Frank Keutsch were supported by the Harvard Solar Geoengineering Research Program and the Simons Foundation (grant no. SFI-MPS-SRM-00005223). Timofei Sukhodolov acknowledges the support from the Swiss National Science Foundation (grant no. 200020E_219166) and the Karbacher Fonds in Graubünden, Switzerland. Gabriel Chiodo, Timofei Sukhodolov and Beiping Luo also have been supported by the Simons Foundation (SFI-MPS-SRM-00005208). Georgios Kelesidis acknowledges the support from the Particle Technology Laboratory, ETH Zurich and, in part, the Swiss National Science Foundation (grant no. 200020_182668, 250320_163243, and 206021_170729). Simulations have been performed at the EULER cluster of ETH Zurich.

Author contributions

Sandro Vattioni wrote the paper draft, created figures, developed the model, tested the model and did data analysis. Rahel Weber performed some of the simulations, created some of the figures and provided support with data analysis. Aryeh Feinberg and Andrea Stenke contributed to model code development, debugging and sanity checking. John A. Dykema performed the Mie-calculations to get the optical properties for alumina and calcite particles and their agglomerates. Beiping Luo and Georgios A. Kelesidis helped with the implementation of microphysics such as the contact angle on solid particles as well as implementation of optical properties. Sandro Vattioni, Thomas Peter, Gabriel Chiodo, Timofei Sukhodolov and Frank N. Keutsch edited the manuscript. Gabriel Chiodo and Thomas Peter supervised Sandro Vattioni. All authors, including Christof Vockenhuber, Markus Ammann and Markus Döbeli contributed to the discussion of the results and provided feedback on the manuscript.

Competing interests

The authors declare no conflicts of interests.

Additional information

Supplementary information The online version contains supplementary material available at <https://doi.org/10.1038/s43247-025-02038-1>.

Correspondence and requests for materials should be addressed to Sandro Vattioni.

Peer review information *Communications Earth & Environment* thanks Kelly Wanser and the other, anonymous, reviewer(s) for their contribution to the peer review of this work. Primary Handling Editors: Sagar Parajuli and Alice Drinkwater. [A peer review file is available].

Reprints and permissions information is available at <http://www.nature.com/reprints>

Publisher's note Springer Nature remains neutral with regard to jurisdictional claims in published maps and institutional affiliations.

Open Access This article is licensed under a Creative Commons Attribution-NonCommercial-NoDerivatives 4.0 International License, which permits any non-commercial use, sharing, distribution and reproduction in any medium or format, as long as you give appropriate credit to the original author(s) and the source, provide a link to the Creative Commons licence, and indicate if you modified the licensed material. You do not have permission under this licence to share adapted material derived from this article or parts of it. The images or other third party material in this article are included in the article's Creative Commons licence, unless indicated otherwise in a credit line to the material. If material is not included in the article's Creative Commons licence and your intended use is not permitted by statutory regulation or exceeds the permitted use, you will need to obtain permission directly from the copyright holder. To view a copy of this licence, visit <http://creativecommons.org/licenses/by-nc-nd/4.0/>.

© The Author(s) 2025

¹Institute of Atmospheric and Climate Science, ETH Zürich, Zurich, ZH, Switzerland. ²John A. Paulson School of Engineering and Applied Sciences, Harvard University, Cambridge, MA, USA. ³Institute for Biogeochemistry and Pollutant Dynamics, ETH Zürich, Zurich, ZH, Switzerland. ⁴Swiss Federal Institute of Aquatic Science and Technology, EAWAG, Dübendorf, ZH, Switzerland. ⁵Physikalisch-Meteorologisches Observatorium Davos/World Radiation Center, PMOD/WRC, Davos, GR, Switzerland. ⁶Department of Chemistry and Chemical Biology, Harvard University, Cambridge, MA, USA. ⁷Department of Earth and Planetary Sciences, Harvard University, Harvard University, Cambridge, MA, USA. ⁸Laboratory of Atmospheric Chemistry, PSI Center for Energy and Environmental Sciences, Paul Scherrer Institute, Villigen, AG, Switzerland. ⁹Laboratory of Ion Beam Physics, ETH Zürich, Zurich, ZH, Switzerland. ¹⁰Particle technology laboratory, Institute of Energy and Process Engineering, ETH Zürich, Zurich, ZH, Switzerland. ¹¹Present address: Federal Office of Meteorology and Climatology, MeteoSwiss, Kloten, ZH, Switzerland. ¹²Present address: Department of Atmospheric Chemistry and Climate, Institute of Physical Chemistry Blas Cabrera, CSIC, Madrid, Spain. ¹³Present address: Faculty of Aerospace Engineering, Delft University of Technology, Delft, HS, The Netherlands. ¹⁴Present address: Instituto de Geociencias (IGEO), CSIC-UCM, Madrid, Spain.

✉ e-mail: sandro.vattioni@env.ethz.ch